Journal

Nature Geoscience (Up to 3000 words. Abs. 180–200 words, 50 references, 4 Figs, max 6)

Title

Damp to super-hydrous magmas recorded by arc root cumulates

Authors

B. M. Urann[1,2,3*], V. Le Roux[2], O. Jagoutz[4], O. Müntener[5], M. D. Behn[6], E. J. Chin[7]

[1] MIT-WHOI Joint Program, Marine Geology and Geophysics, Woods Hole Oceanographic Institution, Woods Hole, MA, USA
[2] Geology and Geophysics Department, Woods Hole Oceanographic Institution, Woods Hole, MA, USA
[3] Department of Geology and Geophysics, University of Wyoming, Laramie, WY, USA
[4] Department of Earth, Atmospheric, and Planetary Sciences, Massachusetts Institute of Technology, Cambridge, MA, USA
[5]Institute of Earth Sciences, University of Lausanne, CH-1015, Lausanne, Switzerland
[6] Department of Earth and Environmental Sciences, Boston College, Chestnut Hill, MA, USA
[7] Geosciences Research Division, Scripps Institution of Oceanography, University of California San Diego, La Jolla, CA, USA

*Now at the University of Wyoming. email: burann@uwyo.edu

Abstract

Magmatic volatiles (e.g., H_2O) are abundant in arc melts and exert fundamental controls on magma evolution, eruption dynamics, and the formation of economic ore deposits. To constrain the H_2O content of arc magmas, most studies have relied on measuring extrusive products and mineral-hosted melt inclusions. However, these methods have inherent limitations that obfuscate the full range of H_2O in arc magmas. Here, we report secondary ion mass spectrometry measurements of volatile (H_2O, F, P, S, Cl) abundances in lower-crustal cumulate minerals from the Kohistan paleo-arc (NW Pakistan), and determine H_2O abundances of melts from which the cumulates crystallized. Pyroxenes retained magmatic H_2O abundances and record damp to hydrous (<1–10 wt.% H_2O) primitive melts. Subsequent crystal fractionation led to formation of super-hydrous melts with ~12–20 wt.% H_2O, predicted petrologically yet never recorded by melt inclusions. Fluid exsolution from super-hydrous melts during ascent is key to porphry copper deposit formation, while foundering of hydrated lower arc crust provides an effective means of transporting hydrogen back into the mantle.

Introduction

Subduction is the primary mechanism of fluid transfer from Earth's surface to the mantle and leads to the generation of volatile-rich arc magmas. Volatile contents (e.g., H_2O, CO_2, S, F, Cl) of arc magmas influence the dynamics of volcanic eruptions, the nature of volcanic gases and magmatic fluids, and the compositional and physical characteristics of arc crust[1]. A major challenge in determining the range of H_2O abundances in arc melts is that H_2O solubility in basaltic melts decreases with decreasing pressure, from >20 wt.% H_2O at 1 GPa and 1200°C[2] to 0.1 wt.% at 1 atmosphere. As a result of this strong pressure dependence on volatile solubility, most arc magmas reach volatile saturation and exsolve volatiles during their ascent through arc crust. To circumvent the effects of volatile loss before and during eruption, workers have relied on melt inclusions entrapped in olivine and clinopyroxene (cpx) phenocrysts[3,4]. Melt inclusions have been interpreted to preserve the H_2O content of arc magmas at depth where olivine crystallized[4], yielding a range of 1.3–7.15 wt.% H_2O (melt Mg# 39–82; molar Mg/(Mg+Fe))[5]. However, subsequent studies have demonstrated that diffusive re-equilibration of hydrogen in melt inclusions is fast (days to hours)[6-8], and therefore melt inclusions may not record the initial H_2O content of arc magmas in the lower arc crust[5,9].

Other approaches to estimate H_2O contents of arc magmas have yielded promising results. Previous workers have shown that arc cumulate minerals may be more reliable indicators of magma hydration state at H_2O contents above ~8 wt.% than melt inclusions. Phase equilibria studies of cumulate amphibole suggest H_2O concentrations up to 10–15 wt.%[10-12], while plagioclase compositional phase equilibria calculations indicate melts up to 9 wt.% H_2O[13]. Similar thermodynamic and experimental approaches at Mount Pinotubo[14], the west-central Mexico volcanic belt[15], and the porphyry copper-rich Gangdese magmatic belt[16] (southern Tibet) have implicated the presence of super-hydrous (>10 wt.% H_2O) magmas. Combined approaches of experimental petrology and electrical conductivity have also inferred the presence super-hydrous magmas with >8 wt.% H_2O in andesitic melts beneath the central Andes and Cascades[17]. Results from these studies suggest that arc magmas should contain significantly more H_2O than inferred from melt inclusion measurements. Reconciling these disparate approaches to quantify arc magma H_2O abundances is critical for evaluating the propensity of copper porphyry formation, which is thought to result from exsolution of hydrous, Cl-rich magmas[18].

Here we build on the arc cumulate approach to explore the H_2O content of primitive and evolved arc magmas by *in-situ* geochemical techniques. Lower-crustal cumulates typically crystallize at 20–50 km depth, prior to H_2O saturation, exsolution, and degassing at shallower levels. We present secondary ion mass spectrometry measurements of volatile abundances (H_2O, F, P, S, Cl) in cumulate minerals (clinopyroxene ± orthopyroxene, garnet, amphibole) from the Kohistan lower arc crust. New volatile, major, and trace element data on mineral phases are combined with petrological models and experimentally calibrated partition coefficients[19] to determine the compositional evolution (and in particular H_2O abundances) of the silicate melts from which the cumulates crystallized. This approach provides a fruitful avenue to determine the range of H_2O abundances in arc melts, from primitive to evolved compositions.

Lower-crustal cumulates from the Kohistan arc terrane

The Cretaceous Kohistan paleo-arc terrane, exposed in the western part of the Himalaya Mountain range (NW Pakistan, Supplementary Figure 1) is a near-complete section of volcanic, plutonic, and upper mantle rocks obducted 50 Ma ago onto India[20] . The Kohistan lower crust can be differentiated into two domains: the Jijal Complex at the stratigraphic base (1.5–0.5 GPa, and the Chilas Complex, obliquely situated above (0.6–0.7 GPa)[21]. Primitive Chilas samples crystallized at c.a. 1200°C[22] and preserve primary igneous textures and compositions on the cm-scale[23] whereas for Jijal crystallization and equilibration temperatures were likely lower based on T_{REE} (Supplementary Table 1) and experimental constraints[24,25]. The two complexes are composed of a suite of plutonic rocks that crystallized either from hydrous (> 4 wt. % H_2O) or damp (< 2 wt.% H_2O) primitive liquids in the Jijal and Chilas complexes, respectively, each following a distinct liquid line of descent (LLD) during differentiation[22,26]. Chilas formed during a period of magmatism at ~80–85 Ma[27], while Jijal magmatism is thought to have been prolonged, beginning at c. 120 Ma[28] with cessation and exhumation of the complex at ~80 Ma[29]. Jijal exemplifies a typical calc-alkaline (i.e., iron depletion trend) differentiation series, whereas Chilas typifies an intermediate to arc tholeiitic arc series[24].

Here we investigated three fresh (<5% alteration) gabbronorites from the Chilas Complex (C7, C48, C66) that were previously studied petrologically[22]. Detailed sample descriptions and locations are provided in the Supplement. Mineral assemblages and compositions of the Chilas gabbronorites indicate that the plutonic rocks crystallized from a common parental magma that evolved along a damp LLD[22]. Sample C66, an olivine gabbronorite, is the most primitive sample investigated; C48 and C7 gabbronorites are more evolved and crystallized from a more fractionated melt than C66[22]. Three minimally altered samples (<5% alteration) were also selected from the Jijal Complex, including two garnet pyroxenites (KK5 and KK8) and a garnet diorite (P05-5A). Field observations and experimental constraints suggest that the Jijal garnet pyroxenites and garnet diorite are broadly related[24] along a hydrous LLD. However, in detail, Jijal samples require individual batches of melt to satisfy field, experimental, and trace element constraints[24]. For example, Jijal garnet diorites yield U-Pb ages of ~92 Ma, whereas garnet pyroxenites formed significantly earlier at 117 ± 7 Ma[27,30]. In addition, Jijal exhibits deviations from experimentally predicted cumulate assemblages, particularly the juxtaposition of pyroxene-garnet hornblendites and garnet hornblende gabbros, suggesting that multiple magmas (likely with different compositions and H_2O contents) were involved in Jijal genesis[24]. As a result, H_2O abundances in the two cumulate series are expected to vary significantly[26].

Preservation of magmatic H_2O abundances in cumulate minerals

In the Chilas gabbronorites, clinopyroxene H_2O abundances range from 152 ± 8 μg/g (2σ) to 1061 ± 399 μg/g (Fig. 1). Orthopyroxene and amphibole were also analyzed in some of the samples, yielding 102–105 μg/g and ~ 2 wt.% H_2O, respectively. In the Jijal samples, clinopyroxene contains from 1770 ± 204 μg/g H_2O to 3900 ± 1000 μg/g H_2O. Garnet and amphibole were also analyzed in some of the samples, yielding 94–167 μg/g

and ~ 1.8 wt.% H_2O, respectively. Data are available in Table 1 and Supplementary Table 2.

Several lines of evidence indicate that magmatic H_2O abundances should have been largely preserved. First, samples are pristine and show no evidence for retrograde overprinting or reaction with metamorphic fluids. This is important because significant loss or addition of hydrogen in nominally anhydrous minerals are often observed in relation with melt[31-33]. Second, only minimal deviations in H_2O abundances are observed at the clinopyroxene rims compared to cores, inconsistent with transient diffusion profiles of hydrogen[31,34] (Supplementary Figure 2). However, hydrogen diffusion length over 1 Ma in clinopyroxene can be >10 m at temperatures of 800–1200°C[33,35], so that hydrogen may have internally re-equilibrated between mineral phases during sub-solidus re-equilibration[36]. Few constraints exist on the effects of sub-solidus re-equilibration of H_2O in lower-crustal lithologies. Nonetheless, H_2O inter-mineral partition coefficients between clinopyroxene and garnet measured in Jijal samples (Supplementary Figure 3) are consistent with experimental partitioning data at magmatic temperatures (>1000°C). The distribution of H_2O between orthopyroxene and clinopyroxene in Chilas samples is similar to what has been observed in other pyroxenites but cannot be compared directly to experiments due to differences in mineralogy (see Supplement for details on inter-mineral partitioning). Lastly, there is no reverse Mg# zoning in pyroxenes, nor major or trace element rim enrichment that would indicate post crystallization modification of pyroxene chemistry by late interstitial liquid. Pyroxenes adjacent to amphibole rims have similar H_2O abundances to others. Therefore, mineral H_2O abundances likely reflect preservation of magmatic H_2O contents at the time of crystallization, with cores largely unaffected by diffusive reequilibration. The same arguments apply for other volatile elements (i.e., fluorine and chlorine), although their diffusivities are likely lower based on their larger ionic radii.

Kohistan's tectonic history may have been crucial in preserving near-magmatic H_2O abundances. Evidence from xenoliths highlights the potential for diffusive H_2O loss during magmatic eruptions, where rapid pressure changes and steep geochemical gradients lead to host-magma degassing, xenolith re-equilibration, and H_2O loss[35] visible in both olivine and pyroxene at temperatures below 900 °C[34]. In Kohistan, the absence of late fluid metasomatism episodes after cumulate formation, followed by rapid exhumation at ~80–85 Ma may have contributed to H_2O preservation.

H_2O and halogen abundances in Kohistan parental melts

Preservation of magmatic H_2O abundances in lower-crustal minerals permits the calculation of H_2O abundances in the parental melts from which the cumulates formed at lower-crustal depths. Partition coefficients for hydrogen between clinopyroxene and melt at relevant *P-T* conditions have been calibrated empirically from experimental studies[19] and range here from 0.0096 to 0.0199 (Table 1). The most primitive Chilas olivine gabbronorite, C66, yields a parental melt H_2O concentration of 1.21 ± 0.09 wt.% (2SE, n=9). More differentiated samples C48 and C7 are in equilibrium with more hydrous melt compositions with 6.38 ± 0.96 (2SE, n=3) and 10.95 ± 4.09 (2SE, n=6) wt.% H_2O, respectively (Fig. 2). The Jijal garnet pyroxenites KK5 and KK8 yield parental melt H_2O concentrations of 8.44 ± 0.39 (2SE, n=5) and 12.44 ± 0.34 (2SE, n=6) wt.%, respectively,

and garnet diorite P05-5A is in equilibrium with a melt that contained 19.6 ± 1.5 wt.% H_2O (2SE, n=5) (Fig. 2). In addition, calculated F and Cl abundances (Table 1) in super-hydrous melts match the highest halogen abundances recorded by melt inclusions (Fig. 2), suggesting that H_2O is lost from melt inclusions compared to halogens.

Crystal fractionation controls H_2O abundances

The large variability in H_2O abundances measured in cumulate minerals and calculated for the melts in equilibrium with the cumulates can be explained by examining correlations between H_2O and other trace and major elements. During crystallization, H_2O preferentially remains in the melt phase and is incompatible in clinopyroxene[37]. In Chilas, clinopyroxene H_2O abundances increase from the most primitive sample C66 (cpx Mg# 81.8) to progressively more evolved C48 (cpx Mg# 78.9) and C7 (cpx Mg# 77.8) (Fig. 1). In addition, H_2O in clinopyroxene positively correlates with other incompatible elements, such as Ce (and all other rare-earth elements), Zr, F (Fig. 3), Na (Fig. 1), and Ti (Supplementary Fig. 4). Ba and Li concentrations may be higher with increasing cpx H_2O. Sr and H_2O correlate negatively due to the presence of plagioclase (Fig. 3). Plagioclase anorthite content (An#, atomic Ca/(Ca+Na)) in C66 (An#89.8), C48 (An# 75.0) and C7 (An# 56.4) also displays a negative correlation with clinopyroxene H_2O abundances, consistent with crystal fractionation. Finally, an equilibrium crystallization model[22] for melt Sr/Y ratio (fluid-mobile/fluid-immobile element) and H_2O concentration links the gabbronorite suite from the most primitive sample (C66) to more evolved compositions (C48 and C7) through a single LLD[22] (Fig. 4A; Supplement). Therefore, increasing H_2O abundances in Chilas pyroxenes and parental melts reflect increasing degrees of crystal fractionation from a single primitive melt. The fit between the data and the model also reinforces the hypothesis that H_2O concentrations in clinopyroxene are near-magmatic.

In the Jijal samples, clinopyroxene H_2O abundances also increase from the two garnet pyroxenites (Mg# 76.2–81.5) to the more evolved P05-5A garnet diorite (Mg# 70.7). P05-5A has the highest Na clinopyroxene content of the series, consistent with its more evolved nature. Unlike Chilas, the Jijal sample series does not exhibit compelling correlations between H_2O and most other incompatible elements due to the fact that Jijal cumulates were derived from individual batches of melt[24], and that elements such as high-field strength elements and REEs were taken up by accessory phases, e.g., ilmenite, zircon, and apatite (Supplementary Figure 5). Nonetheless, H_2O positively correlates with fluid-mobile elements F, Ba and Li in Jijal clinopyroxene (Supplementary Figure 5). In addition, the calculated Sr/Y and H_2O variability of parental melts in equilibrium with Jijal cumulates is consistent with fractional crystallization[22] of individual batches of melts with varying initial H_2O abundances (Fig. 4B), and precipitation of garnet where Y is compatible. Therefore, H_2O variations in Jijal minerals likely reflect varying degrees of crystal fractionation from distinct primitive melts.

Damp to super-hydrous primitive arc melts

The H_2O abundances of primitive melts before extensive crystal fractionation can be back-calculated, assuming that H_2O degassing before cumulate formation was negligible. The solubility of H_2O in basaltic melts at 0.4–0.6 GPa is thought to be ~7–11

wt.%[38,39] and increases with increasing pressure to 20.6 ± 0.9 wt.% H_2O (2σ) at 1 GPa and 1200°C[2]. Barometry estimates of 0.6–0.7 GPa for Chilas and 0.8–1.5 GPa for Jijal, therefore, suggest that equilibrium melts were likely H_2O-undersaturated and did not degas before cumulate crystallization.

To constrain the H_2O contents of primitive melts for the Chilas complex, an additional fractionation correction is needed (see Supplement). Based on previous studies[22], it is assumed that parental liquids in equilibrium with the most primitive gabbronorite (C66) were already evolved with an Mg# of ~53 and underwent 30–50% olivine and clinopyroxene fractionation prior to C66 crystallization. After applying this additional fractionation correction, primitive Chilas melts are inferred to contain 0.61–0.85 wt.% H_2O. This range is consistent with primitive tholeiitic melts formed by decompression melting in an intra-arc extensional setting, i.e., a damp basaltic parental magma with a minor slab contribution[22,26,40].

Similar to the Chilas complex, Jijal cumulates also formed from melts that underwent prior crystallization. Because of the complexity of Jijal, two independent approaches are used to evaluate H_2O concentrations in primitive melts (see Supplement). The first method is based on comparison with crystallization sequences from laboratory experiments, where melts have undergone between 35 and 60% fractional crystallization of olivine and pyroxene prior to amphibole and garnet saturation[24,25]. As H_2O is highly incompatible in both pyroxene and olivine, this correction is rather insensitive to mineral modes and partition coefficients and yields H_2O abundances in Jijal primitive melts of 3.4–8.0 wt.% H_2O for KK5 and KK8. This method cannot be used to evaluate P05-5A, due to its evolved nature. The second method is based on a quantitative petrogenetic model of the Jijal liquid line of descent[41], which permits us to explore a range of initial H_2O abundances for each sample (Fig. 5). The presence of moderately fractionated amphibole-bearing garnet pyroxenites in the fractionation sequence as modeled by previous studies[41] places a lower bound on initial melt H_2O abundances of ~3.25 wt.%. Modeling results are consistent with primitive melt H_2O abundances of ~4–5 wt.% for P05-5A and 6–10 wt.% for KK5 and KK8 (Fig. 5). These values support input from a hydrous slab component during flux melting in a mantle wedge[26].

Implications for ore deposit formation, continental crust, and H_2O fluxes in arcs

Our results show that primitive arc magmas may contain ~0.6–10 wt.% H_2O and reach H_2O saturation of ~20 wt.% H_2O after extensive crystal fractionation in the lower arc crust with Cl abundances up to several thousand μg/g (Fig. 5, Table 1). The estimated H_2O concentrations in primitive arc magmas from this study are more variable and significantly higher than the average of 4 wt. % previously inferred from olivine and clinopyroxene-hosted melt inclusions[5] (Figures 2 and 5B), and support the presence of damp to super-hydrous melts in arc settings[10-12]. The occurrence of super-hydrous, Cl-rich melts under arc roots is important for understanding the formation of ore deposits. Upon magma ascent, H_2O solubility decreases to ~7 wt.% at 0.5 Gpa and 950°C for a basaltic composition (~12 wt.% for rhyolite)[42], leading to exsolution of a Cl-rich fluid phase[43]. Exsolved fluids, thought to be important in porphyry Cu, Mo and Au deposit formation[44-46], may be a natural consequence of H_2O exsolution by fractionated, super-hydrous magmas

at mid-crustal depths. Such a process is substantiated by mass balance calculations[47], phase equilibria modeling[16], and crystallization experiments[14], all of which implicate H_2O-rich melts (> 10 wt.%) in the formation of porphyry copper deposits, where exsolution may initiate in the mid-crust. Future work will require parameterizing Cl partitioning behavior between nominally anhydrous minerals and melt, as copper extraction efficiency during exsolution is highly sensitive to melt Cl concentrations[18].

The andesitic average bulk composition of continental crust may also, in part, be an eventuality of super-hydrous magmas. Crystallization of such magmas at the base of arc crust drives precipitation of thick plagioclase-free, ultramafic sequences, which are seismically indistinguishable from ambient lithospheric mantle[48-51]. Thus, average bulk continental crust estimates using seismic Moho thresholds effectively shift to more evolved (i.e., andesitic) compositions[52,53]. Finally, foundering of hydrated lower arc crust will deliver H_2O fluxes back to the mantle and impact global volatile cycling. The hydrated lower arc crust can therefore modulate volatile cycling between the crust and mantle.

References Cited

1 Wallace, P. J., Plank, T., Edmonds, M. & Hauri, E. H. in *The encyclopedia of volcanoes* 163-183 (Elsevier, 2015).

2 Mitchell, A. L., Gaetani, G. A., O'leary, J. A. & Hauri, E. H. H 2 O solubility in basalt at upper mantle conditions. *Contrib Mineral Petr* **172**, 85 (2017).

3 Dobson, P. F., Skogby, H. & Rossman, G. R. Water in boninite glass and coexisting orthopyroxene: concentration and partitioning. *Contrib Mineral Petr* **118**, 414-419 (1995).

4 Sisson, T. & Layne, G. H2O in basalt and basaltic andesite glass inclusions from four subduction-related volcanoes. *Earth Planet Sc Lett* **117**, 619-635 (1993).

5 Plank, T., Kelley, K. A., Zimmer, M. M., Hauri, E. H. & Wallace, P. J. Why do mafic arc magmas contain~ 4 wt% water on average? *Earth Planet Sc Lett* **364**, 168-179 (2013).

6 Gaetani, G. A., O'Leary, J. A., Shimizu, N., Bucholz, C. E. & Newville, M. Rapid reequilibration of H2O and oxygen fugacity in olivine-hosted melt inclusions. *Geology* **40**, 915-918 (2012).

7 Portnyagin, M., Almeev, R., Matveev, S. & Holtz, F. Experimental evidence for rapid water exchange between melt inclusions in olivine and host magma. *Earth Planet Sc Lett* **272**, 541-552 (2008).

8 Bucholz, C. E., Gaetani, G. A., Behn, M. D. & Shimizu, N. Post-entrapment modification of volatiles and oxygen fugacity in olivine-hosted melt inclusions. *Earth Planet Sc Lett* **374**, 145-155 (2013).

9 Annen, C., Blundy, J. & Sparks, R. The genesis of intermediate and silicic magmas in deep crustal hot zones. *J Petrol* **47**, 505-539 (2006).

10 Goltz, A. E., Krawczynski, M. J., Gavrilenko, M., Gorbach, N. V. & Ruprecht, P. Evidence for superhydrous primitive arc magmas from mafic enclaves at Shiveluch volcano, Kamchatka. *Contrib Mineral Petr* **175**, 1-26 (2020).

11 Grove, T. L. *et al.* Magnesian andesite and dacite lavas from Mt. Shasta, northern California: products of fractional crystallization of H 2 O-rich mantle melts. *Contrib Mineral Petr* **148**, 542-565 (2005).
12 Krawczynski, M. J., Grove, T. L. & Behrens, H. Amphibole stability in primitive arc magmas: effects of temperature, H 2 O content, and oxygen fugacity. *Contrib Mineral Petr* **164**, 317-339 (2012).
13 Zellmer, G. F. *et al.* Petrogenesis of antecryst-bearing arc basalts from the Trans-Mexican Volcanic Belt: Insights into along-arc variations in magma-mush ponding depths, H2O contents, and surface heat flux. *Am Mineral* **101**, 2405-2422 (2016).
14 Prouteau, G. & Scaillet, B. Experimental constraints on the origin of the 1991 Pinatubo dacite. *J Petrol* **44**, 2203-2241 (2003).
15 Carmichael, I. S. The andesite aqueduct: perspectives on the evolution of intermediate magmatism in west-central (105–99 W) Mexico. *Contrib Mineral Petr* **143**, 641-663 (2002).
16 Lu, Y.-J., Loucks, R. R., Fiorentini, M. L., Yang, Z.-M. & Hou, Z.-Q. Fluid flux melting generated postcollisional high Sr/Y copper ore–forming water-rich magmas in Tibet. *Geology* **43**, 583-586 (2015).
17 Laumonier, M., Gaillard, F., Muir, D., Blundy, J. & Unsworth, M. Giant magmatic water reservoirs at mid-crustal depth inferred from electrical conductivity and the growth of the continental crust. *Earth Planet Sc Lett* **457**, 173-180 (2017).
18 Tattitch, B., Chelle-Michou, C., Blundy, J. & Loucks, R. R. Chemical feedbacks during magma degassing control chlorine partitioning and metal extraction in volcanic arcs. *Nature communications* **12**, 1-11 (2021).
19 O'Leary, J. A., Gaetani, G. A. & Hauri, E. H. The effect of tetrahedral Al3+ on the partitioning of water between clinopyroxene and silicate melt. *Earth Planet Sc Lett* **297**, 111-120 (2010).
20 Tahirkheli, R. A. K. & Jan, M. Q. Geology of Kohistan, Karakorum Himalaya, northern Pakistan. *Special issue of the Geological Bulletin of the University of Peshawar, Pakistan* **11**, 1-30 (1979).
21 Jagoutz, O. & Schmidt, M. W. The formation and bulk composition of modern juvenile continental crust: The Kohistan arc. *Chem Geol* **298**, 79-96 (2012).
22 Jagoutz, O. *et al.* Petrology and mineral chemistry of lower crustal intrusions: the Chilas Complex, Kohistan (NW Pakistan). *J Petrol* **48**, 1895-1953 (2007).
23 Loucks, R. R. Restoration of the elemental and stable-isotopic compositions of diffusionally altered minerals in slowly cooled rocks. *Contrib Mineral Petr* **124**, 346-358 (1996).
24 Müntener, O. & Ulmer, P. Arc crust formation and differentiation constrained by experimental petrology. *American Journal of Science* **318**, 64-89 (2018).
25 Ulmer, P., Kaegi, R. & Müntener, O. Experimentally derived intermediate to silica-rich arc magmas by fractional and equilibrium crystallization at 1· 0 GPa: An evaluation of phase relationships, compositions, liquid lines of descent and oxygen fugacity. *J Petrol* **59**, 11-58 (2018).
26 Jagoutz, O., Muntener, O., Schmidt, M. W. & Burg, J. P. The roles of flux- and decompression melting and their respective fractionation lines for

continental crust formation: Evidence from the Kohistan arc. *Earth Planet Sc Lett* **303**, 25-36, doi:10.1016/j.epsl.2010.12.017 (2011).

27 Schaltegger, U., Zeilinger, G., Frank, M. & Burg, J. P. Multiple mantle sources during island arc magmatism: U–Pb and Hf isotopic evidence from the Kohistan arc complex, Pakistan. *Terra Nova* **14**, 461-468 (2002).

28 Bouilhol, P., Jagoutz, O., Hanchar, J. M. & Dudas, F. O. Dating the India–Eurasia collision through arc magmatic records. *Earth Planet Sc Lett* **366**, 163-175 (2013).

29 Burg, J. P., Jagoutz, O., Dawood, H. & Hussain, S. S. Precollision tilt of crustal blocks in rifted island arcs: structural evidence from the Kohistan Arc. *Tectonics* **25** (2006).

30 Dhuime, B. *et al.* Multistage evolution of the Jijal ultramafic–mafic complex (Kohistan, N Pakistan): implications for building the roots of island arcs. *Earth Planet Sc Lett* **261**, 179-200 (2007).

31 Demouchy, S., Jacobsen, S. D., Gaillard, F. & Stern, C. R. Rapid magma ascent recorded by water diffusion profiles in mantle olivine. *Geology* **34**, 429-432 (2006).

32 Le Roux, V. *et al.* Postmelting hydrogen enrichment in the oceanic lithosphere. *Science Advances* **7**, eabf6071, doi:10.1126/sciadv.abf6071 (2021).

33 Peslier, A. H. & Luhr, J. F. Hydrogen loss from olivines in mantle xenoliths from Simcoe (USA) and Mexico: Mafic alkalic magma ascent rates and water budget of the sub-continental lithosphere. *Earth Planet Sc Lett* **242**, 302-319 (2006).

34 Xu, Y. *et al.* Reconciling the discrepancy between the dehydration rates in mantle olivine and pyroxene during xenolith emplacement. *Geochim Cosmochim Ac* **267**, 179-195 (2019).

35 Ferriss, E., Plank, T. & Walker, D. Site-specific hydrogen diffusion rates during clinopyroxene dehydration. *Contrib Mineral Petr* **171**, 55 (2016).

36 Schaffer, L. A. *et al.* Effects of melting, subduction-related metasomatism, and sub-solidus equilibration on the distribution of water contents in the mantle beneath the Rio Grande Rift. *Geochim Cosmochim Ac* **266**, 351-381 (2019).

37 Hauri, E. H., Gaetani, G. A. & Green, T. H. Partitioning of water during melting of the Earth's upper mantle at H2O-undersaturated conditions. *Earth Planet Sc Lett* **248**, 715-734 (2006).

38 Berndt, J. *et al.* A combined rapid-quench and H2-membrane setup for internally heated pressure vessels: Description and application for water solubility in basaltic melts. *Am Mineral* **87**, 1717-1726 (2002).

39 Hamilton, D., Burnham, C. W. & Osborn, E. The solubility of water and effects of oxygen fugacity and water content on crystallization in mafic magmas. *J Petrol* **5**, 21-39 (1964).

40 Jagoutz, O., Müntener, O., Burg, J.-P., Ulmer, P. & Jagoutz, E. Lower continental crust formation through focused flow in km-scale melt conduits: The zoned ultramafic bodies of the Chilas Complex in the Kohistan island arc (NW Pakistan). *Earth Planet Sc Lett* **242**, 320-342 (2006).

41 Jagoutz, O. E. Construction of the granitoid crust of an island arc. Part II: a quantitative petrogenetic model. *Contrib Mineral Petr* **160**, 359-381, doi:10.1007/s00410-009-0482-6 (2010).
42 Newman, S. & Lowenstern, J. B. VolatileCalc: a silicate melt–H2O–CO2 solution model written in Visual Basic for excel. *Computers & Geosciences* **28**, 597-604 (2002).
43 Alletti, M. *et al.* Chlorine partitioning between a basaltic melt and H2O–CO2 fluids at Mount Etna. *Chem Geol* **263**, 37-50 (2009).
44 Lee, C.-T. A. & Tang, M. How to make porphyry copper deposits. *Earth Planet Sc Lett* **529**, 115868 (2020).
45 Hedenquist, J. W., Arribas, A. & Reynolds, T. J. Evolution of an intrusion-centered hydrothermal system; Far Southeast-Lepanto porphyry and epithermal Cu-Au deposits, Philippines. *Economic Geology* **93**, 373-404 (1998).
46 Rezeau, H. & Jagoutz, O. The importance of H2O in arc magmas for the formation of porphyry Cu deposits. *Ore Geology Reviews* **126**, 103744 (2020).
47 Klemm, L. M., Pettke, T. & Heinrich, C. A. Fluid and source magma evolution of the Questa porphyry Mo deposit, New Mexico, USA. *Mineralium Deposita* **43**, 533 (2008).
48 Loucks, R. R. Deep entrapment of buoyant magmas by orogenic tectonic stress: Its role in producing continental crust, adakites, and porphyry copper deposits. *Earth-Science Reviews* **220**, 103744 (2021).
49 Kodaira, S. *et al.* Seismological evidence for variable growth of crust along the Izu intraoceanic arc. *Journal of Geophysical Research: Solid Earth* **112** (2007).
50 Kodaira, S. *et al.* New seismological constraints on growth of continental crust in the Izu-Bonin intra-oceanic arc. *Geology* **35**, 1031-1034 (2007).
51 Behn, M. D. & Kelemen, P. B. Stability of arc lower crust: Insights from the Talkeetna arc section, south central Alaska, and the seismic structure of modern arcs. *Journal of Geophysical Research: Solid Earth* **111** (2006).
52 O'Reilly, S. Y. & Griffin, W. Moho vs crust–mantle boundary: evolution of an idea. *Tectonophysics* **609**, 535-546 (2013).
53 Müntener, O. & Ulmer, P. Experimentally derived high‐pressure cumulates from hydrous arc magmas and consequences for the seismic velocity structure of lower arc crust. *Geophysical Research Letters* **33** (2006).

Corresponding Author
Ben Urann, burann@uwyo.edu

Acknowledgements
We thank Brian Monteleone and Neel Chatterjee for their technical expertise on the Cameca 1280 at the Northeast National Ion Microprobe Facility at WHOI and electron microprobe at MIT, respectively. We thank S. Parman, W.J. Collins and R. Loucks for their constructive comments which improved the manuscript.

Contributions

BU conceived the study, BU and VLR collected and interpreted the data, and wrote the manuscript. OJ and OM provided samples, data, and geochemical models. BU, VLR, MB, and EC acquired financial support. All authors contributed to editing the manuscript.

Funding Statement

Funding for this study was supported by the Woods Hole Oceanographic Institution Ocean Venture Fund to BMU, NSF awards EAR-P&G #1839128 and EAR-P&G/Geophysics #1855302 to VLR, and EAR-18-55430 to MDB and EJC. VLR also acknowledges the support from the Visiting Scholar at SCIENCE program at the University of Copenhagen, Denmark. BMU also acknowledges continued support from NSF OCE Post-doctoral Research Fellow grant (#2126559).

Data Availability Statement

All data which support the findings of this study are presented herein, or cited in the text and Methods. Olivine-hosted arc melt inclusion data for Figure 5B was downloaded from the Georoc Database (http://georoc.mpch-mainz.gwdg.de/georoc/).

Code Availability Statement

Code used in the generation of figures is available by request.

472 **Figures**

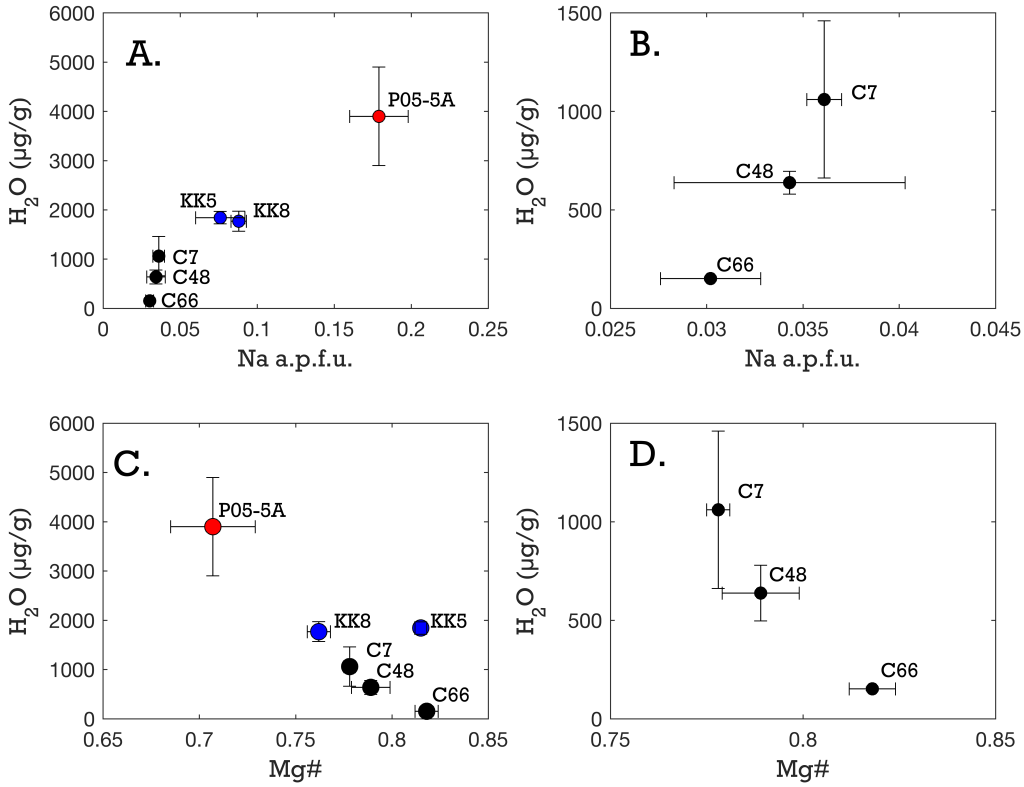

473

474 Figure 1. Clinopyroxene H_2O abundances plotted against major element compositions in
475 clinopyroxene for the both the Jijal and Chilas (A. and C.) and Chilas only (B. and
476 D.). Panels A. and B. show octahedrally coordinated Na in atoms per formula unit,
477 panels C. and D. Mg# (molar Mg/(Mg+Fe)). Error bars are 2SE of the mean.

478

479

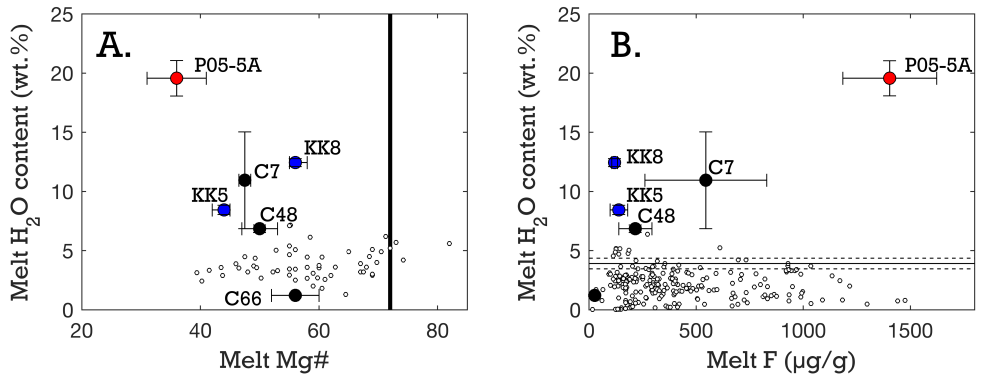

480

481 **Figure 2. A.** Equilibrium melt H_2O abundances plotted against melt Mg#. Melt Mg#
482 inferred from clinopyroxene Mg# for both Chilas (black circles) and Jijal (blue and red
483 circles) cumulates. Mg# error bars denote highest and lowest measured cpx Mg# for each
484 sample, H_2O error bars are 2SE of the mean. Melt inclusion literature data (white circles)
485 are maximum water abundances for individual arc volcanoes[5] converted from olivine
486 forsterite content to melt Mg#. Thick vertical black line denotes Mg# of melts in
487 equilibrium with mantle olivine Fo_{90} (i.e., Mg# 72). **B**. Fluorine and H_2O abundances of
488 arc melt inclusions (See Methods for relevant citations) compared to parental melts
489 calculated for Kohistan. Horizontal line signifies mean H_2O content of arc melts (dashed
490 lines are 1 s.d.) as interpreted from melt inclusions[5].

491

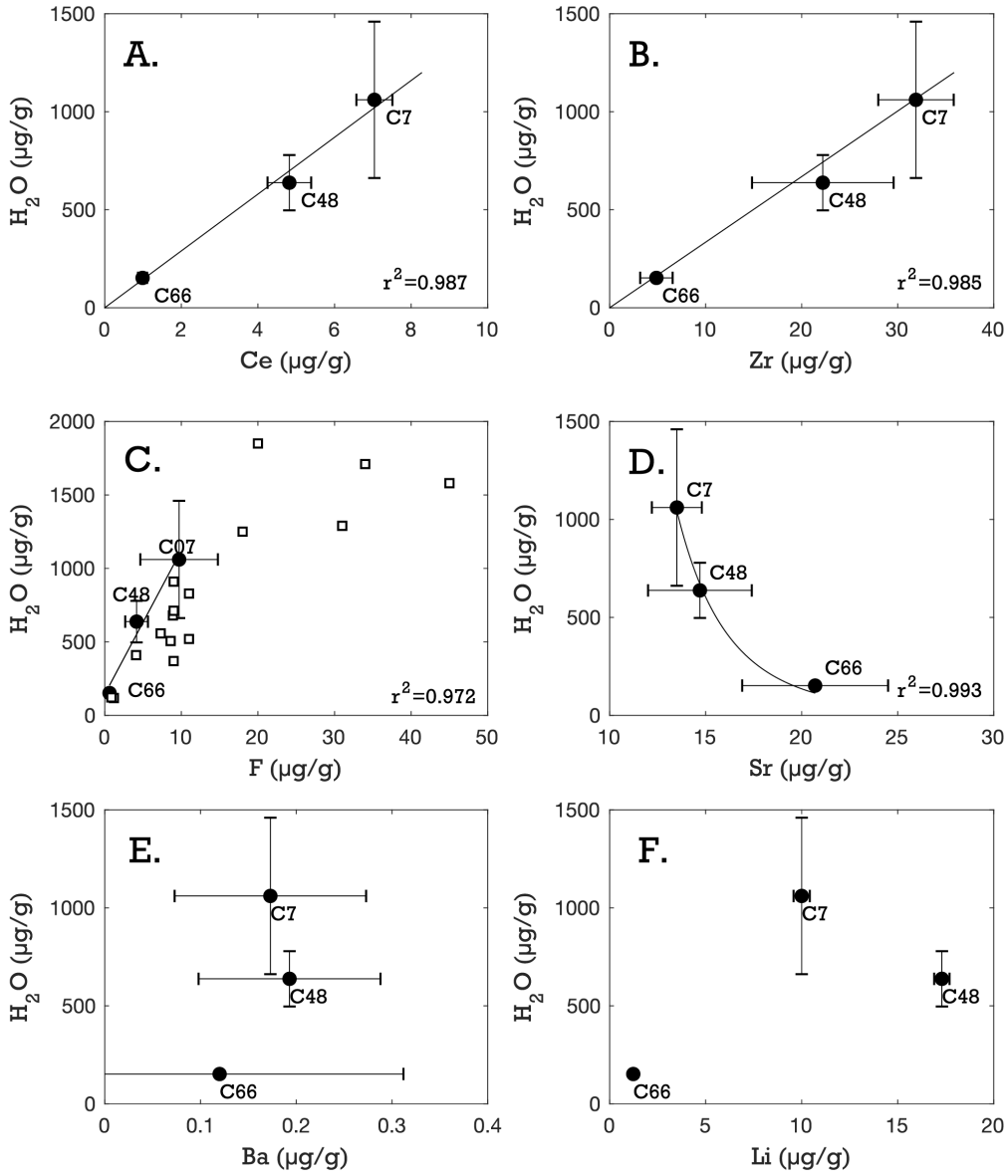

492

493 Figure 3. Chilas clinopyroxene H_2O concentrations plotted against trace element
494 concentrations with various geochemical affinities. Plots show: the rare earth element Ce
495 (A.), the high field strength element Zr (B.), the volatile halogen F (C.) and the fluid
496 mobile elements Sr (D.), Ba (E.) and Li (F.). Concentrations are the mean of each
497 sample (clinopyroxene cores only for H_2O). Error bars are two standard error of the
498 mean. White squares denote experimental partitioning data from the literature[19,37]. Black
499 solid lines and curves denote best fit slopes calculated using MATLAB functions poly1
500 (A., B. and C.) and power1 (D.).

501

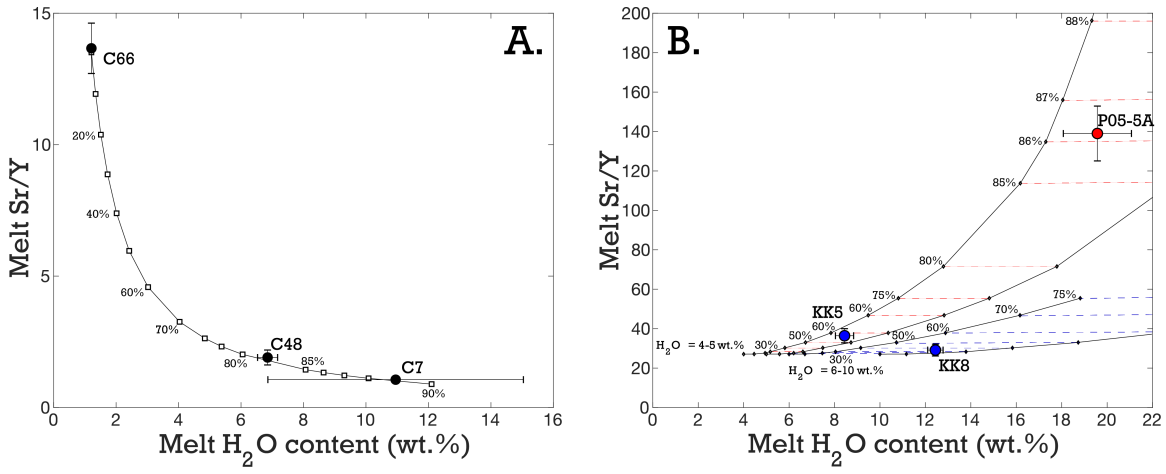

Figure 4. Crystallization models for both Chilas (A.) and Jijal (B.). **A.** Equilibrium crystallization model (white squares) for Chilas gabbronorites showing the evolution of Sr/Y ratios against H_2O abundances in melts. Upon continued crystallization of plagioclase, Sr decreases as it is compatible in plagioclase, whereas Y increases, being incompatible in all crystallizing phases. Values along curves are percent crystallization. Parental melt has an H_2O concentration of 1.21 wt.% and is the melt parental to C66. **B.** Fractional crystallization models[41] for Jijal cumulates showing the evolution of Sr/Y ratios against varying H_2O abundances in melts. The fitted range of H_2O contents in parental melts varies from 4 to 10 wt.% H_2O. Dashed blue and red lines are tie lines connecting identical extents of crystallization for different starting melt H_2O abundances. For details of the two models, see Supplement.

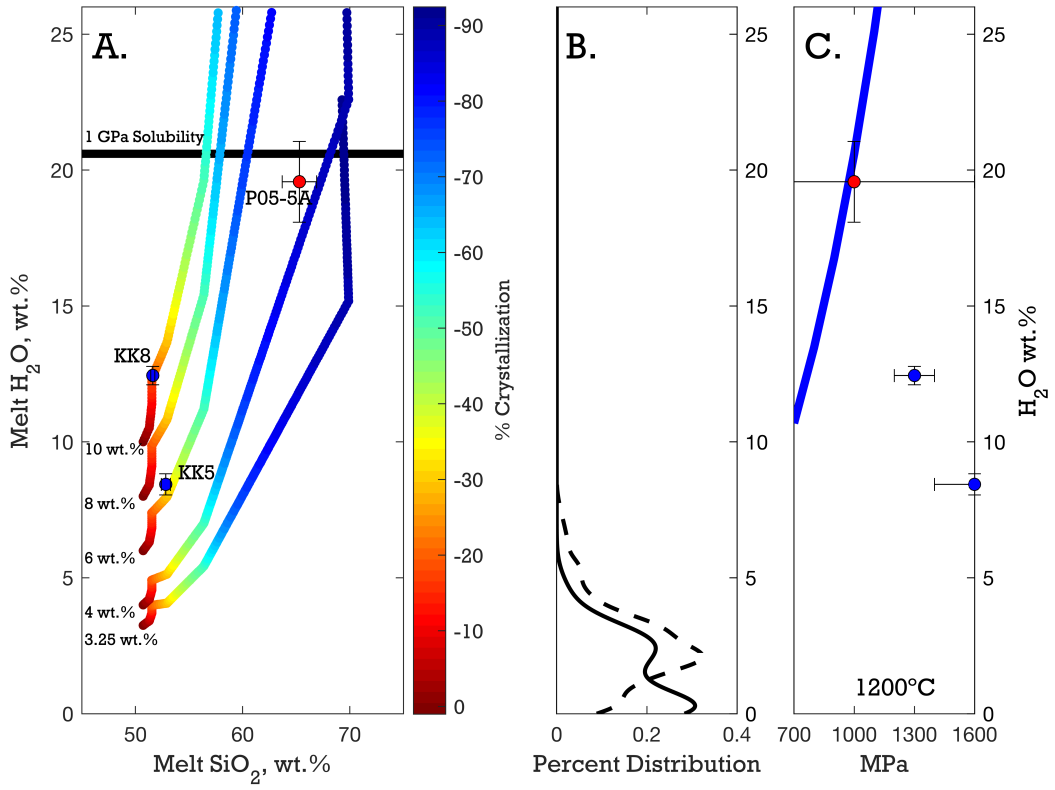

Figure 5. A. Jijal melt crystallization model based on published petrogenetic model[41]. Equilibrium melt SiO_2 content for each sample calculated based on clinopyroxene Mg# using modeled liquid line of descent. Thick black line denotes 1 GPa H_2O solubility for a basaltic melt[2]. Silicic magmas tend to have higher water solubilities than basalt, however constraints at relevant *P-T* conditions are lacking. Values next to each curve represent the range of H_2O abundances in parental melts, with the lower bound constrained by the minimum amount of water needed to crystallize amphibole in the fractionation sequence[41], i.e. 3.25 wt.% H_2O. See Supplement for details. B. Probability density function of olivine-hosted arc melt inclusions from the Georoc Database (http://georoc.mpch-mainz.gwdg.de/georoc/). Primitive melt inclusions (Mg#>65) shown as a solid back line (n=171). Melt inclusions with Mg# of 35 to 65 (n=879), similar to the Mg# calculated for Kohistan parental melts, are shown as a dashed black line. Primitive melt inclusions (solid black line) display two probability peaks at 0.3 and 2.3 wt.% H_2O with a maximum H_2O of 4.8 wt.%, whereas those with an Mg# of 35 to 65 show a single peak at 2.0 wt.% H_2O and a maximum of 7.5 wt.% H_2O. C. H_2O solubility curve for basaltic melts at 1200°C[2] compared to H_2O abundances in Jijal cumulates at various *P*.